



Observations of infrared radiative cooling in the thermosphere on daily to multiyear timescales from the TIMED/SABER instrument

Martin G. Mlynczak,¹ Linda A. Hunt,² B. Thomas Marshall,³ F. Javier Martin-Torres,⁴ Christopher J. Mertens,¹ James M. Russell III,⁵ Ellis E. Remsberg,¹ Manuel López-Puertas,⁶ Richard Picard,⁷ Jeremy Winick,⁷ Peter Wintersteiner,⁸ R. Earl Thompson,³ and Larry L. Gordley³

Received 30 July 2009; revised 23 September 2009; accepted 22 October 2009; published 24 March 2010.

[1] We present observations of the infrared radiative cooling by carbon dioxide (CO₂) and nitric oxide (NO) in Earth's thermosphere. These data have been taken over a period of 7 years by the Sounding of the Atmosphere using Broadband Emission Radiometry (SABER) instrument on the NASA Thermosphere-Ionosphere-Mesosphere Energetics and Dynamics (TIMED) satellite and are the dominant radiative cooling mechanisms for the thermosphere. From the SABER observations we derive vertical profiles of radiative cooling rates (W m⁻³), radiative fluxes (W m⁻²), and radiated power (W). In the period from January 2002 through January 2009, we observe a large decrease in the cooling rates, fluxes, and power consistent with the declining phase of solar cycle 23. The power radiated by NO during 2008 when the Sun exhibited few sunspots was nearly one order of magnitude smaller than the peak power observed shortly after the mission began. Substantial short-term variability in the infrared emissions is also observed throughout the entire mission duration. Radiative cooling rates and radiative fluxes from NO exhibit fundamentally different latitude dependence than do those from CO₂, with the NO fluxes and cooling rates being largest at high latitudes and polar regions. The cooling rates are shown to be derived relatively independent of the collisional and radiative processes that drive the departure from local thermodynamic equilibrium (LTE) in the CO₂ 15 μm and the NO 5.3 μm vibration-rotation bands. The observed NO and CO₂ cooling rates have been compiled into a separate data set and represent a climate data record that is available for use in assessments of radiative cooling in upper atmosphere general circulation models.

Citation: Mlynczak, M. G., et al. (2010), Observations of infrared radiative cooling in the thermosphere on daily to multiyear timescales from the TIMED/SABER instrument, *J. Geophys. Res.*, 115, A03309, doi:10.1029/2009JA014713.

1. Introduction

[2] The terrestrial thermosphere and mesosphere have been the least explored regions of Earth's atmosphere. They are too high for in situ measurements from aircraft or balloons. Rocket or ground-based measurements on a global basis are not practical and do not provide the suite of measurements required for a complete characterization of these

regions. In the middle 1990s, remote sensing technology became sufficiently advanced to enable comprehensive satellite observations of these regions of the atmosphere. The NASA Thermosphere-Ionosphere-Mesosphere Energetics and Dynamics (TIMED) mission was developed to explore the Earth's atmosphere above 60 km altitude and was launched in December 2001. A fundamental goal of the mission is to quantify the energy budget of mesosphere and thermosphere. One of four instruments on the TIMED mission, the Sounding of the Atmosphere using Broadband Emission Radiometry (SABER) instrument, was specifically designed to measure the energy budget of the mesosphere and lower thermosphere [Mlynczak, 1996, 1997].

[3] The SABER instrument is a 10 channel limb scanning radiometer. It scans the Earth's limb continuously recording profiles of infrared radiance (W m⁻² sr⁻¹) from the atmosphere in discrete spectral intervals [Russell et al., 1999]. The specific wavelength bands observed by SABER were

¹NASA Langley Research Center, Hampton, Virginia, USA.

²SSAI, Hampton, Virginia, USA.

³GATS Inc., Newport News, Virginia, USA.

⁴Jet Propulsion Laboratory, California Institute of Technology, Pasadena, California, USA.

⁵Hampton University, Hampton, Virginia, USA.

⁶IAA, Granada, Spain.

⁷AFRL, Hanscom AFB, Bedford, Massachusetts, USA.

⁸ARCON Corp., Waltham, Massachusetts, USA.

chosen so that a variety of data products could be retrieved or derived, including kinetic temperature, ozone, water vapor, carbon dioxide, atomic oxygen, atomic hydrogen, rates of energy deposition, rates of energy loss, and rates of radiative heating and cooling. To this end, SABER measures two of the three key infrared emissions that govern radiative cooling of the atmosphere above 100 km: nitric oxide (NO) at 5.3 μm [Kockarts, 1980] and carbon dioxide (CO_2) at 15 μm [Curtis and Goody, 1956]. The third emission, the fine structure line of atomic oxygen (O^3P) at 63 μm [Bates, 1951] is not measured by SABER but has been observed by the CRISTA instrument that flew twice in the 1990s on the Space Shuttle [Grossman *et al.*, 2000] and by numerous rocket experiments [Grossman and Vollmann, 1997] and even by high-altitude balloons [Mlynczak *et al.*, 2004]. The SABER data set is the first global, long-term, and continuous record of the NO and CO_2 emissions from the thermosphere.

[4] The SABER data set is now 7 years in length and has already provided some basic insight into the heat budget of the thermosphere on a variety of timescales. Mlynczak *et al.* [2003, 2005] have reported the observed nature of the nitric oxide emission in the thermosphere in response to geomagnetic storm events, demonstrating a “thermostat” effect in which the infrared emission rapidly and efficiently removes storm energy deposited into the thermosphere and thus returns it to its original state in a short period of time. The long-term effects of the declining phase of solar cycle 23 were clearly evident in the NO emission in less than 5 years [Mlynczak *et al.*, 2007] and 9 day periodicities in both the NO and CO_2 emissions have been related to the occurrence of coronal holes on the Sun [Mlynczak *et al.*, 2007].

[5] The purpose of this paper is to further examine variability in the NO 5.3 μm and CO_2 15 μm emissions with the SABER data set. In particular, the extent of solar minimum conditions during the end of solar cycle 23 offers a unique opportunity to study the radiative cooling in the thermosphere under exceptionally quiescent conditions. We also examine the infrared emissions as a function of latitude and altitude. In addition, the newest version of the SABER data set (v1.07) is used in this study. Last, the results presented here form a climate data record for the thermosphere useful for assessing general circulation models of the upper atmosphere. The cooling rate data may be obtained from the authors upon request.

[6] In section 2, we review the data processing methodology. In section 3, we present the results in the order of the processing: vertical profiles of radiative cooling (W m^{-3}), fluxes of infrared emission (W m^{-2}), and radiated power (W). Discussions on the fundamentally different roles of cooling by NO and CO_2 are given. In section 4, we discuss the sensitivity of the results to parameters in the SABER retrieval algorithms and in section 5 we give a summary.

2. Derivation of Infrared Parameters

[7] The fundamental SABER measurement is the infrared radiance ($\text{W m}^{-2} \text{sr}^{-1}$) measured in the limb viewing geometry as a function of tangent altitude. The instrument scans the atmosphere from approximately 400 km tangent altitude down to 5 km below the hard Earth surface, recording

an infrared radiance sample every 0.4 km. The NO 5.3 μm emission is observed as high as 300 km during periods of intense geomagnetic storms. The CO_2 15 μm emission is typically observed up to 139 km. Approximately 1400 profiles of infrared emission are obtained for each of the 10 SABER channels in one day. During the limb scan between 100 and 200 km (the nominal range reported in this paper) the TIMED spacecraft moves approximately 1° of latitude. The nominal instantaneous field of view of the instrument is 2 km at the tangent point on the Earth’s limb.

[8] The TIMED satellite is in an orbit inclined 74° with respect to the equator. The SABER instrument views perpendicular to the spacecraft velocity vector. In order to keep the instrument within its allowable range of operating temperatures, the TIMED spacecraft executes a rotation about its yaw axis every 60 days to keep the Sun from illuminating the instrument’s thermal radiator. While in the “northward” viewing mode the instrument views from approximately 83° N to 55° S. After the yaw maneuver the instrument views from approximately 55° N to 83° S. This operational scenario results in the regions between 55° N and 55° S being viewed continuously while the regions above 55° latitude are viewed continuously for two months every other yaw cycle, that is, two months of viewing followed by a two month gap, followed by two months of viewing, etc. This process repeats exactly the same temporal gaps in both hemispheres every year.

[9] In the results below for zonal mean cooling rates and fluxes we present annual averages. Because of the SABER viewing geometry, the averages are over 12 months only between $\pm 55^\circ$ in latitude (corresponding to 82% of atmospheric area). In the regions poleward of 55° we average the six months of available data every year. While not truly annual, these 6 month averages cover locally two months during winter, two months during fall, one month during spring, and one month during summer. There is no obvious discontinuity in the cooling rates and fluxes shown in Figures 1 and 2 below and we believe that the results are substantially representative of the annual behavior, although comparisons with models are required to verify this assertion. More than 50,000 individual cooling rate profiles are observed in a 6 month period poleward of 55° .

[10] The derivation of the infrared radiative cooling rates (W m^{-3}) is accomplished by different techniques for the NO and CO_2 emissions owing to the different opacities of these molecules in the limb view, and to account for the different physical processes that result in emission and cooling of the atmosphere by these molecules. To further study the energy balance, we vertically integrate each profile of radiative cooling to obtain the flux (W m^{-2}) of energy exiting the thermosphere. The fluxes are then zonally integrated to provide an estimate of the equator-to-pole distribution of radiative cooling which is central to the large-scale atmospheric circulation. The fluxes are then integrated with respect to area around a latitude circle, and then, from pole to pole, to estimate the total power (W) radiated each day by the thermosphere. These analysis procedures with SABER data are given in the work of Mlynczak *et al.* [2005]. We will review these here since there are fundamental differences in the approaches for analyzing the (more) optically thick 15 μm band of CO_2 and the optically thin 5.3 μm band of NO.

2.1. NO(v) at 5.3 μm

[11] Infrared emission from NO is a substantial cooling mechanism throughout the thermosphere. Because of the low atmospheric density, the vibration-rotation bands of the NO molecule depart from local thermodynamic equilibrium (LTE) [e.g., *Funke and López-Puertas*, 2000]. The NO vibrational states are excited primarily by collisions with atomic oxygen with a rate coefficient of $4.2 \times 10^{-11} \exp(-2700/T) \text{ cm}^3 \text{ s}^{-1}$ [*Hwang et al.*, 2003], where T is the kinetic temperature. By comparison, excitation by the absorption of terrestrial radiation is several orders of magnitude smaller. Nitric oxide is also formed through a series of chemical reactions that excite high-lying vibration-rotation bands especially during geomagnetic storms. These have been observed near 195 km by the CIRRIS-1A instrument that flew on the Space Shuttle [*Dothe et al.*, 2002; *Sharma et al.*, 1996].

[12] The approach to deriving the NO cooling rates from SABER observations has been discussed by *Mlynczak et al.* [2005], and is reviewed here. The emission from nitric oxide is in the weak line limit of radiative transfer. The equation of radiative transfer describing a transition in the weak line limit is given in the limb view by the expression

$$R(H_o) = \frac{hc\nu}{4\pi} \sum_x V(x) dx, \quad (1)$$

where $R(H_o)$ is the measured spectrally integrated radiance ($\text{W m}^{-2} \text{ sr}^{-1}$) at tangent altitude H_o , h is Planck's constant, c is the speed of light, ν is the frequency of the transition (wave numbers, cm^{-1}), $V(x)$ is the volume emission rate of photons at the tangent altitude, and dx is a path element along the limb line of sight. An Abel or geometric inversion may be applied to the measured radiance profile, assuming spherical symmetry about the tangent point, yielding a vertical profile of the rate of emission of energy per unit volume (W m^{-3}). For optically thin transitions such as those of NO, the energy escapes the thermosphere completely: half of the energy is emitted to space, half to the atmosphere below.

[13] As the SABER instrument is a filter radiometer, the initial result from the Abel inversion process is a cooling/emission rate that is weighted by the filter bandpass of the instrument. To obtain the total rate of emission, a correction factor is applied to the measured in-band emission rate to obtain the emission rate for the entire band. The correction factor varies substantially with altitude for NO and has been computed from extensive model calculations discussed by *Mlynczak et al.* [2005]. The correction factor was verified through observations of NO spectra made by the MIPAS instrument [*Gardner et al.*, 2007] on the Envisat satellite. Surprisingly, *Mlynczak et al.* [2005] found relatively small variation in this correction ("unfilter") factor from quiescent to geomagnetically disturbed conditions.

[14] In the results presented below, we treat the entire emission from NO as cooling the atmosphere. Terrestrial ("earthshine") emission is insignificant as an excitation mechanism of nitric oxide vibrations, relative to collisions with atomic oxygen. The results from *Dothe et al.* [2002] indicate that emission from high-lying NO vibrational levels is still well below that of the fundamental ($v=1$ to $v=0$) band. The correction factor applied to the SABER measured

in-band emission rate accounts for out-of-band contributions of the 2–1 and 3–2 vibrational states as well. Potential refinements to this process will be discussed in section 5.

2.2. CO₂(ν_2) at 15 μm

[15] In this section, we outline the method to compute the cooling rates for the CO₂ 15 μm ν_2 fundamental band transition, with upper state designation CO₂(01¹0). Later in the paper, we will examine the role of cooling by the first hot band in this mode, i.e., the CO₂ (02²0 \rightarrow 01¹0) transition. Above 100 km, the CO₂ 15 μm fundamental band is not exactly optically thin, but neither is it very optically thick. Because of this, derivation of the cooling rates for the CO₂ molecule is not as straightforward as for NO. Specifically, the absence of true weak line radiative transfer precludes application of an Abel or geometric inversion to simply derive a cooling/emission rate profile. In addition, radiative exchange with other layers of the atmosphere occurs, although absorption of radiation from the lower atmosphere is relatively small [*López-Puertas and Taylor*, 2002]. Only emission resulting from collisional excitation results in a cooling of the atmosphere. In addition, because of the opacity, not all emission escapes to space or the atmosphere below, unlike NO. We must therefore employ a technique to compute the true cooling of the atmosphere given these constraints.

[16] The SABER experiment measures emission in the ν_2 bending mode of CO₂ at 15 μm for the purpose of retrieving the kinetic temperature of the atmosphere. The 15 μm bands are also responsible for the radiative cooling of the atmosphere. As with NO, the vibration-rotation bands of carbon dioxide depart from LTE in the upper mesosphere and thermosphere. The SABER temperature derivation includes detailed modeling of the collisional and radiative processes that drive the observed transitions from LTE [*Mertens et al.*, 2002]. Specifically, the Curtis matrix approach [*López-Puertas et al.*, 1986a, 1986b] is employed in the SABER non-LTE modeling and temperature derivation process and directly yields the infrared radiative cooling rates in kelvin per day. These cooling rates computed at each iteration step are output and stored as standard data products upon convergence of the temperature retrieval.

[17] To derive the local rate $\partial Q/\partial t$ of radiative cooling in W m^{-3} for CO₂ at a given altitude we apply the first law of thermodynamics:

$$\frac{\partial Q}{\partial t} = \rho C_p \frac{\partial T}{\partial t}, \quad (2)$$

where C_p is the heat capacity at constant pressure, ρ is the density, and $\partial T/\partial t$ is the derived radiative cooling rate in kelvin per day. From the ideal gas law this can be written as

$$\frac{\partial Q}{\partial t} = \frac{p}{T} \frac{C_p}{R} \frac{\partial T}{\partial t}. \quad (3)$$

[18] In equation (3), R is the gas constant. This approach to computing cooling rates and fluxes was successfully applied in the stratosphere by *Mlynczak et al.* [1999]. In our present analyses, the pressure, temperature, and $\partial T/\partial t$ are obtained from the SABER v1.07 data set. Although the

Nitric Oxide Annual Average Cooling Rate

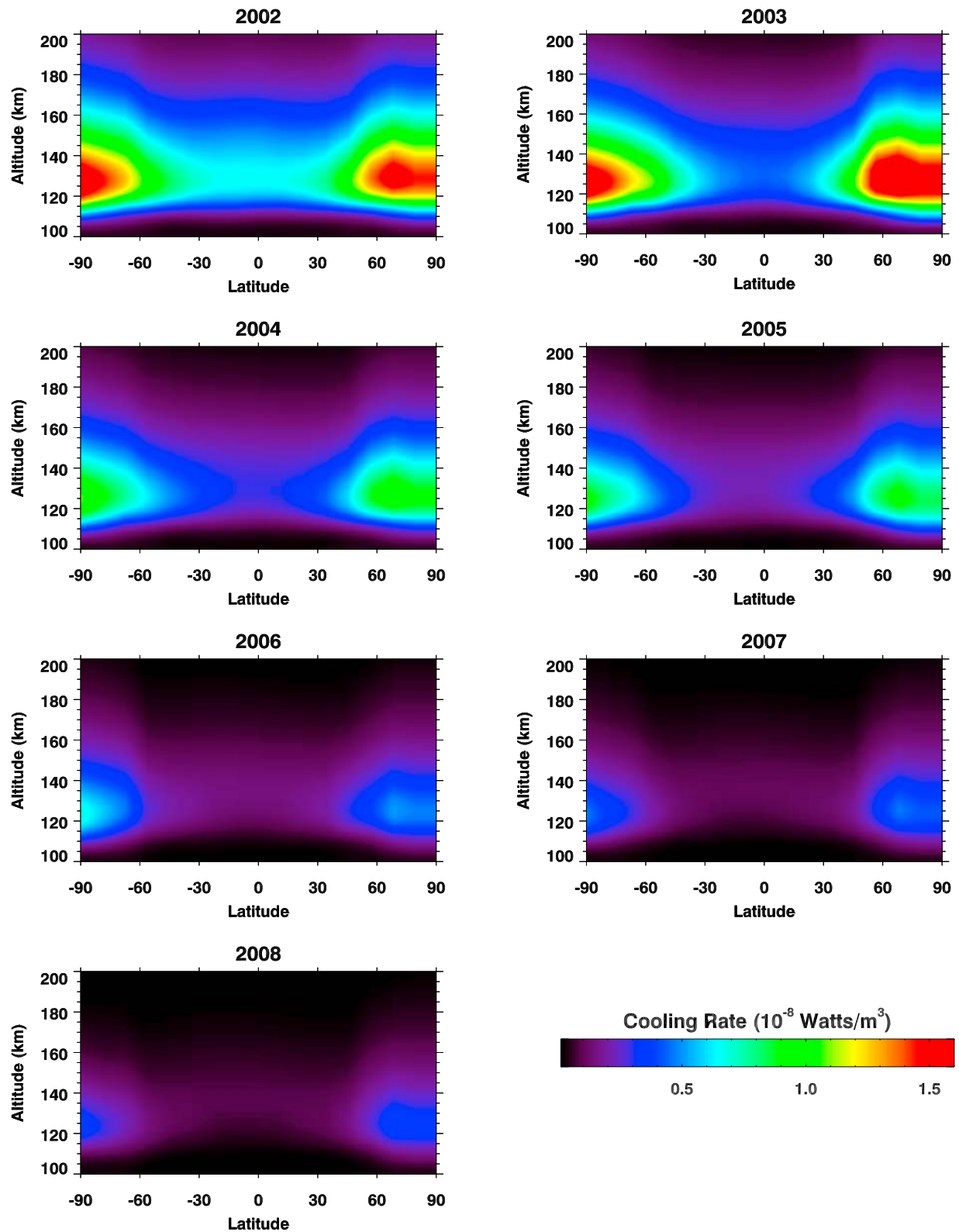


Figure 1. Zonal average, annual mean cooling rates (W m⁻³) for nitric oxide from 2002 through 2008.

Carbon Dioxide Annual Average Cooling Rate

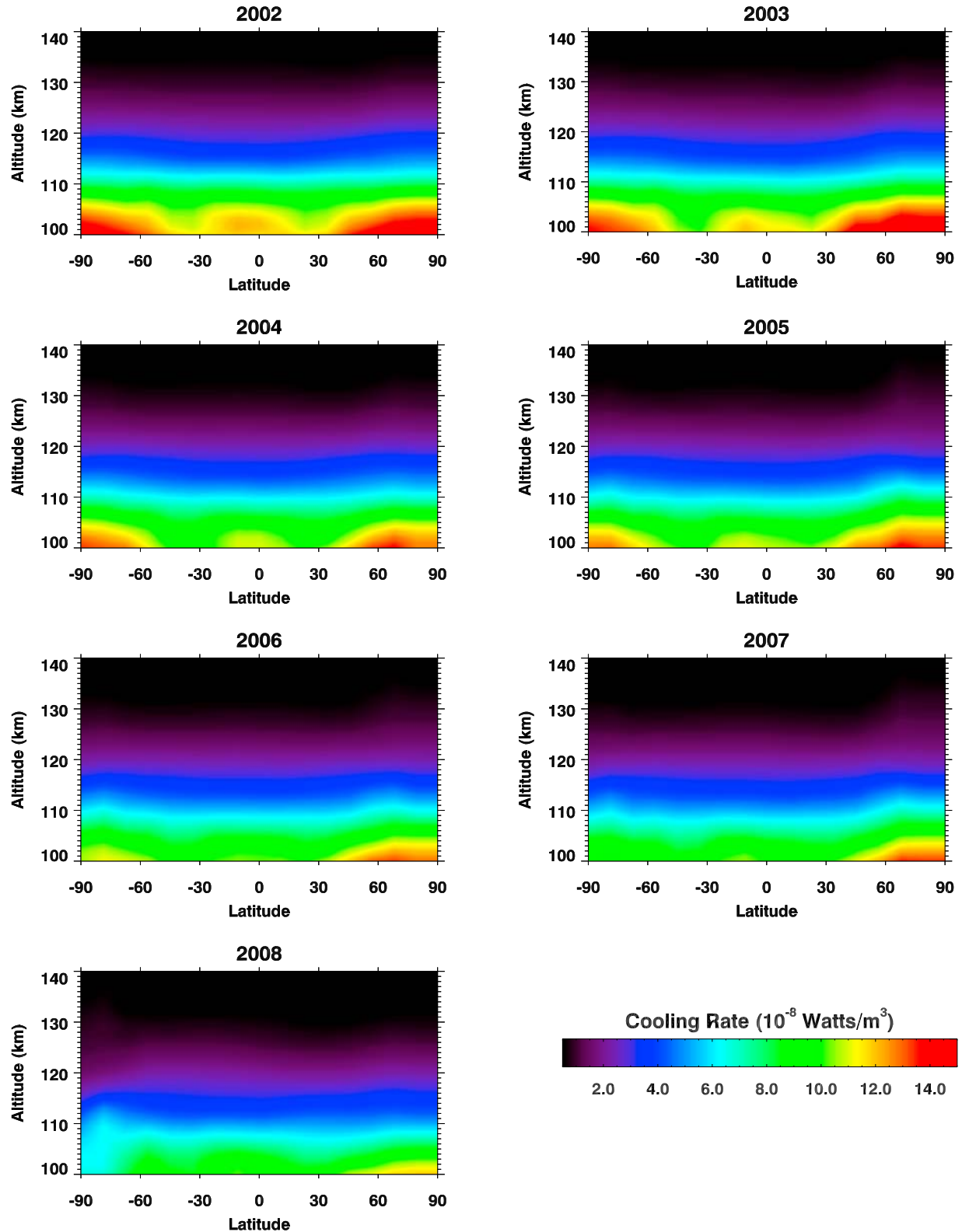


Figure 2. Zonal average, annual mean cooling rates (W m^{-3}) for carbon dioxide from 2002 through 2008.

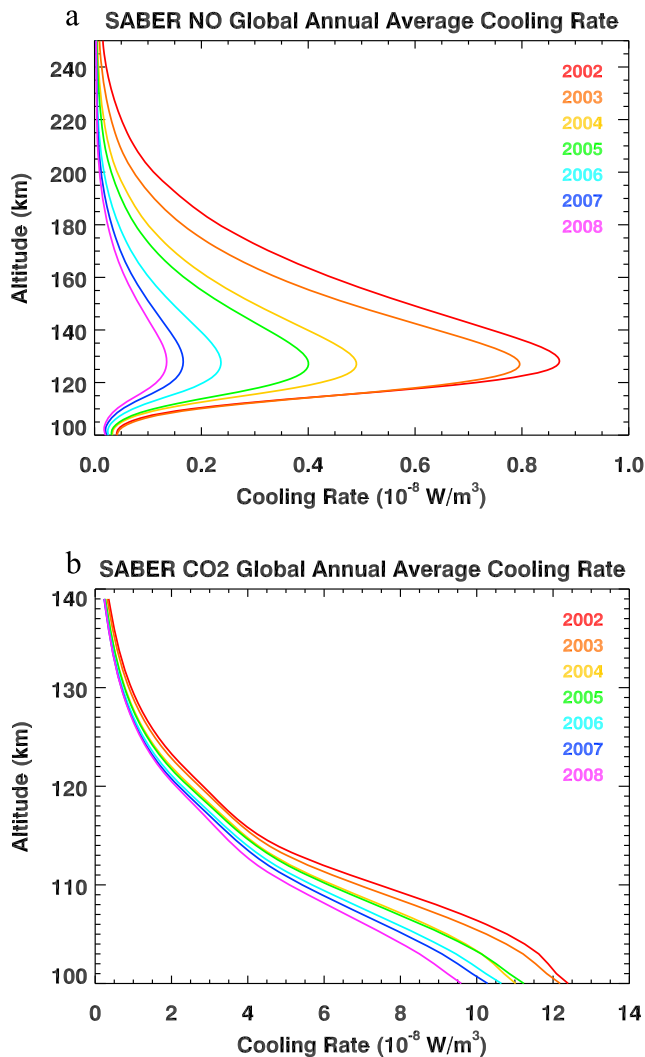


Figure 3. Global annual average cooling rate profiles, solar maximum (2002) and solar minimum (2008), and all years in between for (a) NO, derived from the cooling rates in Figure 1 and (b) CO₂ derived from the cooling rates in Figure 2.

effect is small, we also include the variation of the ratio C_p/R with altitude to be consistent with that used in the SABER data processing, thus accounting for the effects of atomic oxygen on C_p .

3. Results

3.1. Cooling Rates for NO at 5.3 μm

[19] We begin by examining the cooling rates (W m^{-3}) for NO over the 7 years of data to date. The SABER instrument began routine operations in mid-January 2001. To maintain SABER's orientation on the "cold" side of the spacecraft, the TIMED spacecraft undergoes a 180° yaw maneuver every 60 days, as dictated by the progression through local time in the satellite's 74° inclined orbit. Thus in a year the spacecraft executes a series of six yaw maneuvers, allowing the same progression of local time to be repeated each year. In all figures presented below, unless noted otherwise, we

display annual averages for each of the seven "yaw years" that have been observed to date. Each "yaw year" runs from mid-January to the next mid-January. So year 2002 runs from January 2002 to January 2003, and so on.

[20] Shown in Figure 1 are the zonally averaged, annual mean cooling rates in W m^{-3} for NO observed by SABER from January 2002 through January 2009, i.e., yaw years 2002 through 2008. There are two features immediately obvious from the data. First, the maximum cooling rates occur at high latitudes near the poles, implying a strong geomagnetic influence. Second, the magnitude of the cooling rates visibly decreases each year in the series from 2002 through 2008. This decrease is concurrent with the declining phase of solar cycle 23. At the altitude of the cooling rate peak poleward of 60°, the cooling rates decrease by a factor of ~ 4.5 . The cooling rate is observed to decrease throughout the entire range from 100 to 200 km over the 7 years of observations. By 2008, there is very little emission observed by SABER above 180 km.

[21] For carbon dioxide, we find a different picture of cooling rates in the plots shown in Figure 2. Whereas the NO cooling rates showed a clear equator-to-pole enhancement throughout the thermosphere, CO₂ exhibits a relatively small gradient in equator-to-pole cooling above 105 km. Below 105 km there is evidence of strong cooling near the poles and also at the equator. The equatorial enhancement in CO₂ cooling is visible in all 7 years of data. Similar to the NO cooling, a decrease in the strength of the CO₂ cooling over the 7 years is also visible in Figure 2.

[22] Figures 1 and 2 demonstrate a decrease in radiative cooling by NO and CO₂ in the thermosphere over the last 7 years. This decrease is consistent with a decrease in the temperature of the thermosphere which affects both NO and CO₂, although the temperature sensitivity of the NO emission is substantially larger than for CO₂. The strength of radiative cooling is proportional to $\exp(\Delta E/k_B T)$ where ΔE is the photon energy, k_B is Boltzmann's constant, and T is the kinetic temperature. Since ΔE for NO is about 2.8 times larger than for CO₂, NO emission has a substantially larger sensitivity to a specific change in temperature. Decreases in atomic oxygen over the solar cycle also contribute to the decline in infrared cooling from both molecules.

[23] The NO cooling will also be affected directly by a decrease in the NO density that would be expected to occur during the declining phase of the solar cycle, while the CO₂ concentration has only a small anticipated source due to continued anthropogenic buildup and virtually no known sinks that are due to the solar cycle. Thus the larger observed changes in NO cooling as compared to CO₂ are due to a combination of a larger sensitivity of the emission to temperature and to an overall decrease in the NO abundance. The influence of solar cycle on radiative cooling is best shown in Figures 3a and 3b which depict the annual, global average cooling in 2002 through 2008, for NO and CO₂, respectively. For NO in Figure 3a, we have extended the plot up to 250 km altitude, illustrating the extent of nitric oxide emission during solar maximum (and also the sensitivity of the SABER instrument.) The NO cooling shows a continued and marked decrease for each year in the sequence. The largest decrease is in the global average cooling by nitric oxide, approximately a factor of ~ 6.5 at the peak. In contrast, the CO₂ cooling has decreased by about

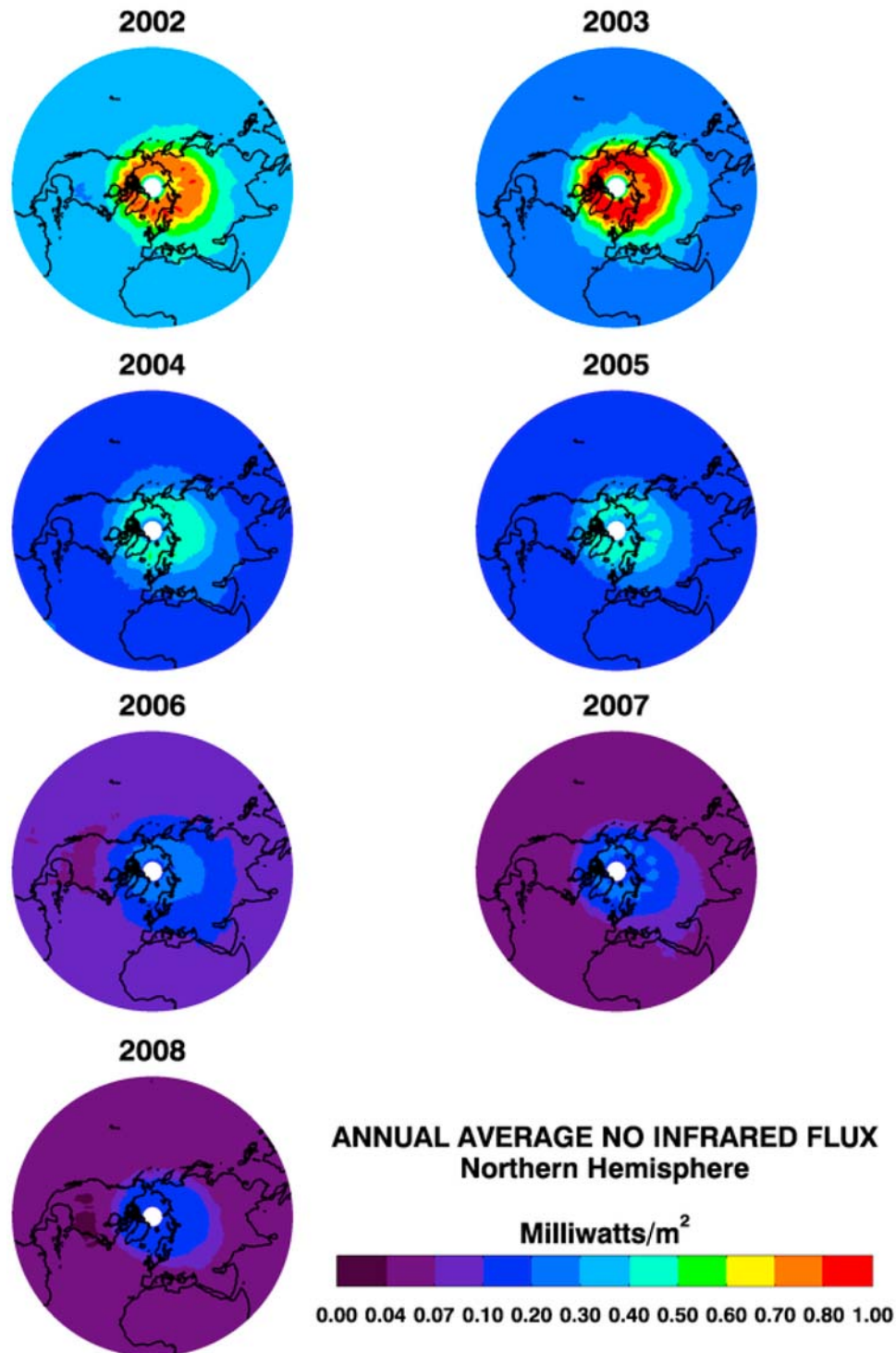


Figure 4. Annual average exiting longwave radiative flux (mW m^{-2}) for nitric oxide in the northern hemisphere from 2002 to 2008.

35% over the solar cycle. The smaller sensitivity of the CO_2 cooling to the solar cycle is due to the fact that the CO_2 emissions originate in the lower (more dense) atmosphere, to the smaller sensitivity of the CO_2 emission to temperature changes, and to a lack of sinks of CO_2 abundance.

3.2. Fluxes of Exiting Longwave Radiation

[24] The next step in the process of assessing the radiative cooling is to integrate vertically the cooling rate profiles and obtain the flux of longwave radiation that exits the thermosphere. We choose to call this the “exiting” longwave

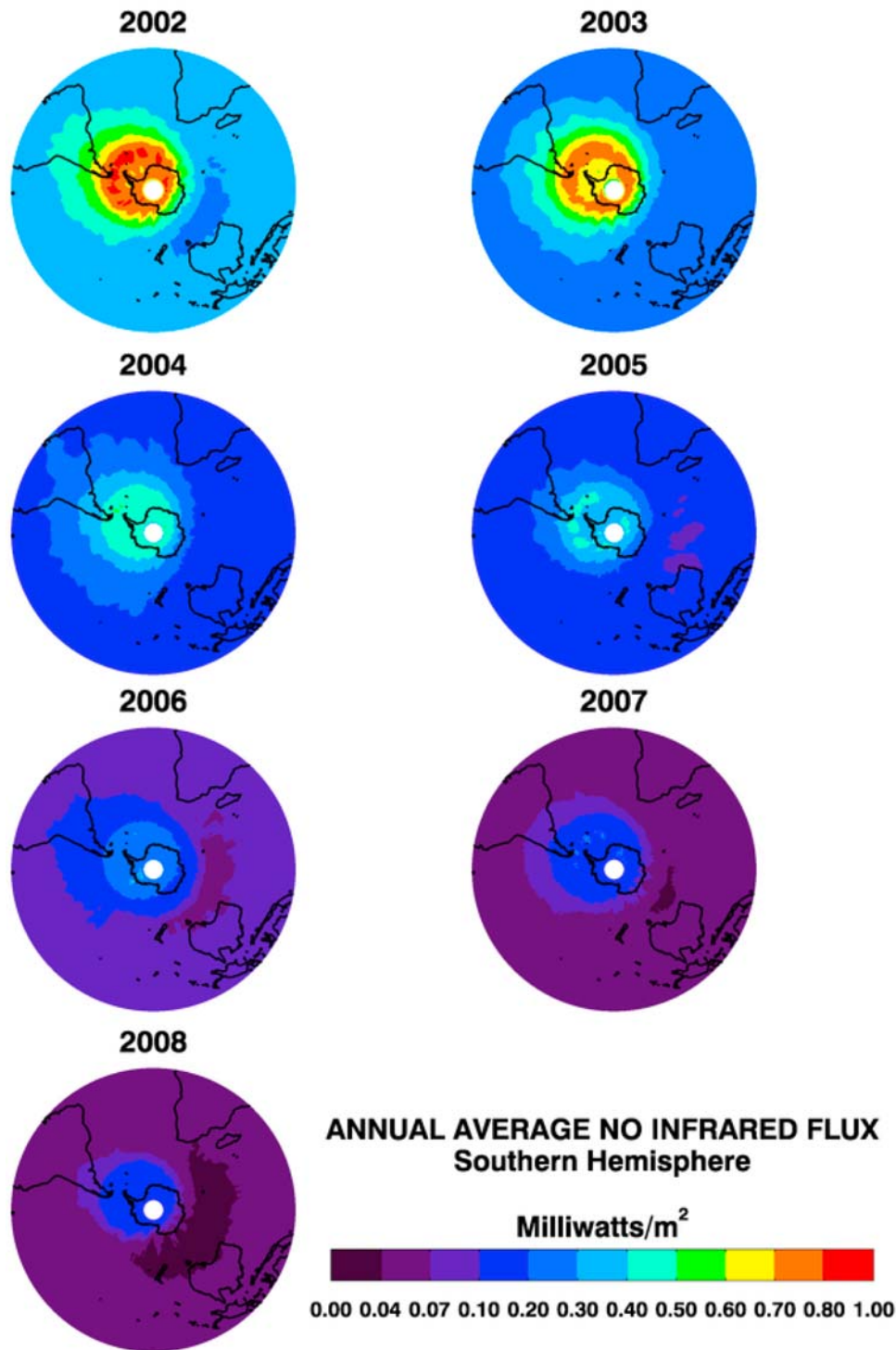


Figure 5. Annual average exiting longwave radiative flux (mW m^{-2}) for nitric oxide in the southern hemisphere from 2002 to 2008.

radiation (ELR) in analogy to the ‘outgoing’ longwave radiation (OLR) used in studies of the Earth’s tropospheric climate. The difference is that the OLR all leaves the planet whereas only about half of the ELR leaves the planet while the rest is absorbed in the atmosphere below the thermosphere. The range of vertical integration is 100 to 200 km for NO and 100 to 139 km for CO_2 .

[25] Shown in Figures 4 and 5 are polar stereographic plots of ELR for NO in the northern and southern hemispheres, respectively. The scale on the color bar runs from 0.0 to 1.0 mW m^{-2} . These ELR plots show the annual average fluxes of radiation exiting the thermosphere between 2002 and 2008 and correspond to the same time periods as the cooling rates shown in Figure 1. Clearly visible are larger

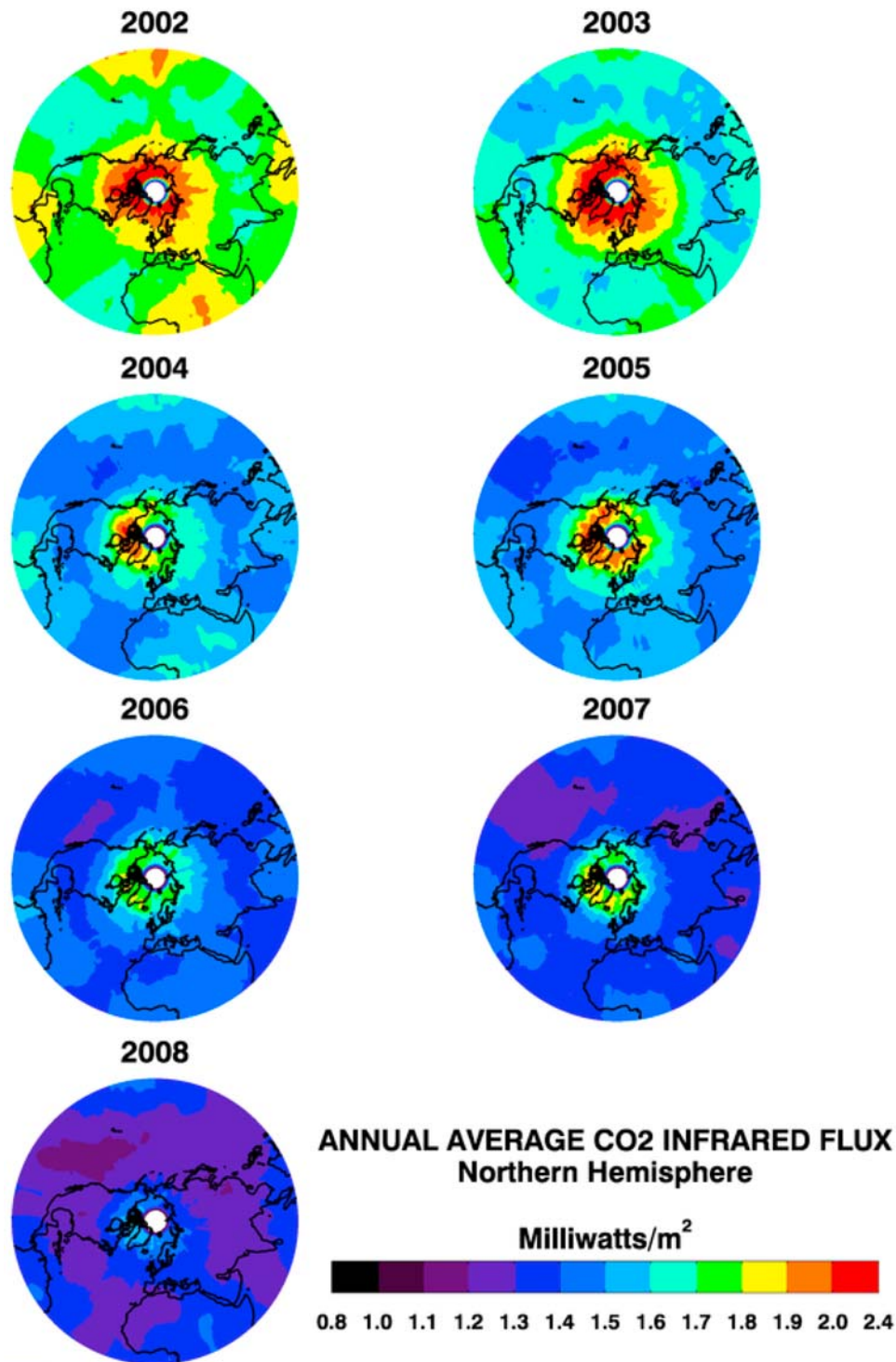


Figure 6. Annual average exiting longwave radiative flux (mW m^{-2}) for carbon dioxide in the northern hemisphere from 2002 to 2008.

fluxes near the poles in all years, with fluxes in 2002 and 2003 peaking in excess of 0.8 mW m^{-2} . Also evident is a dramatic decrease in flux from 2002 to 2008. In 2002, in most of each hemisphere the ELR exceeds 0.3 mW m^{-2} . In 2008 the ELR over most of the globe is well below 0.07 mW m^{-2} . Thus the effect of the declining phase of solar cycle 23 is clearly evident in the ELR.

[26] Figures 6 and 7 show the ELR for the northern and southern hemispheres from 2002 to 2008 for CO_2 . The scale runs from 0.8 to 2.4 mW m^{-2} . The CO_2 fluxes are substantially larger than those for NO and are reflective of the role CO_2 plays in cooling the lower (and more dense) thermosphere. Evident in Figures 6 and 7 is a general decrease from 2002 to 2008. However, as evidenced by the

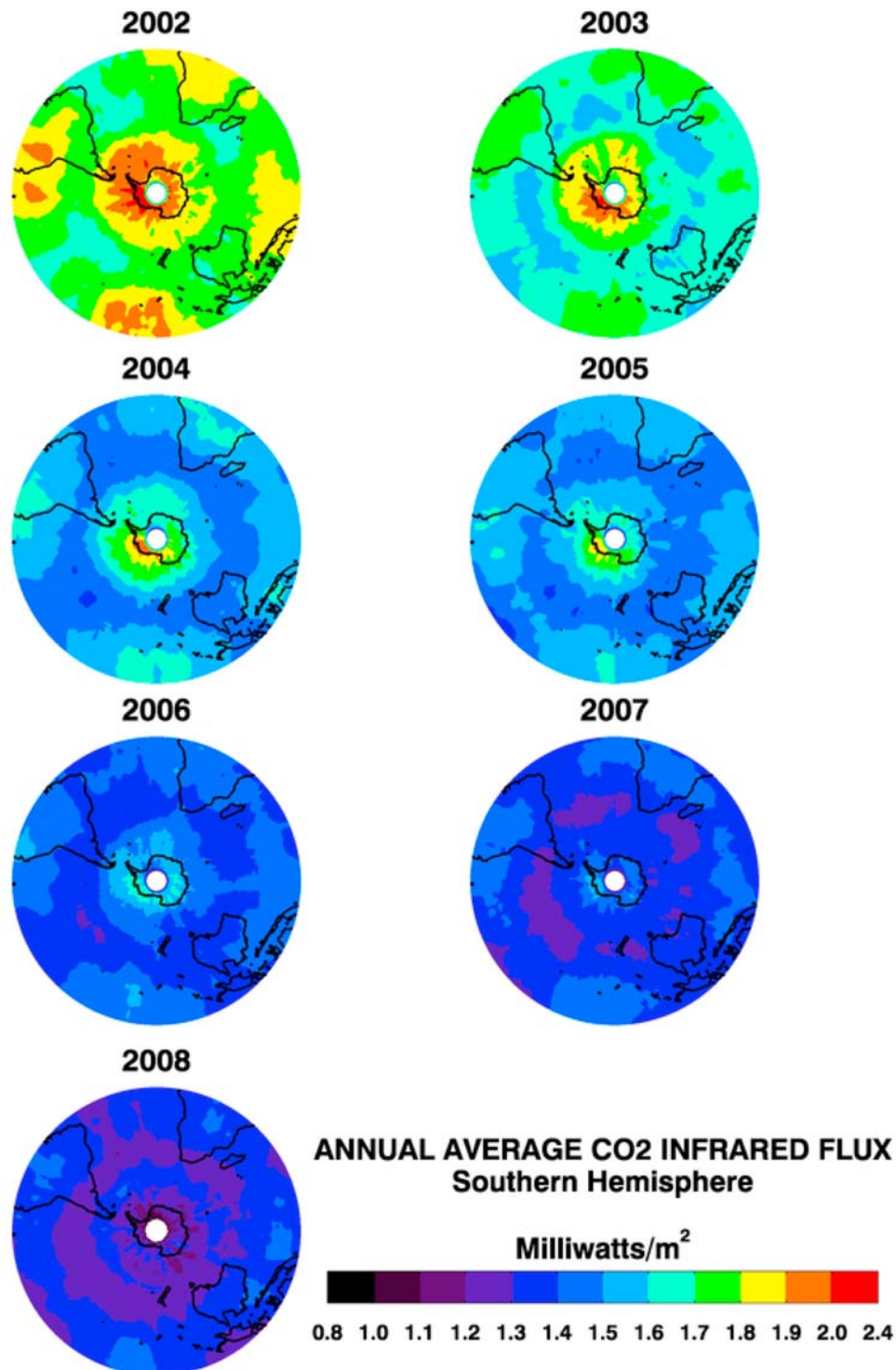


Figure 7. Annual average exiting longwave radiative flux (mW m^{-2}) for carbon dioxide in the southern hemisphere from 2002 to 2008.

emission rates of energy in Figures 2 and 3b, the decrease in the ELR for CO_2 is much less than that for NO , on a percentage basis. As with the NO emission, the CO_2 ELR is always largest in polar regions, reflecting the high-latitude enhancements in CO_2 cooling shown in Figure 2 in the lower thermosphere. The tropical enhancement in cooling by CO_2 shown in Figure 2 is also evident in the fluxes in Figures 6

and 7. The tropical enhancement in fact exhibits four alternating maxima and minima in each year, perhaps implying a dynamical (tidal?) effect. The tropical maximum decreases substantially from solar maximum in 2002 to solar minimum in 2008. The extent of large fluxes of ELR from CO_2 also decreases at the pole, but there is still substantial cooling, although over a reduced area, in 2008.

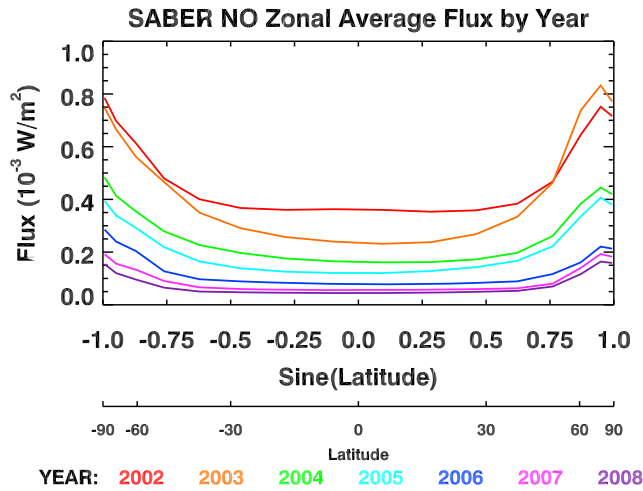


Figure 8. Annual mean, zonal average exiting longwave radiative flux (W m^{-2}) for nitric oxide from 2002 to 2008.

3.3. Zonal Mean Fluxes of Exiting Longwave Radiation

[27] Next, we zonally average the ELR for NO and CO_2 shown in Figures 4–7 to display the annual average ELR as a function of latitude. In Figures 8 and 9, we show the annual average ELR for each year 2002 through 2008 for NO and CO_2 , respectively. The ELR is plotted versus the sine of latitude so that the abscissa is proportional to atmospheric area. The first feature that stands out from examination of Figures 8 and 9 is that starting in 2003, the ELR decreases each year compared to the previous year. The decrease is generally uniform with latitude although the ELR in the high-latitude northern hemisphere in 2003 is comparable to that in 2002, and again comparable in 2004 and 2005. The ELR for NO decreases by about a factor of 8 in the low to mid-latitudes, while the ELR for CO_2 decreases by about 30% over the same range of latitudes. The general decrease in ELR from 2002 to 2008 is again an indication of the effects of the declining phase of solar cycle 23. However, the fact that the ELR decrease is not identical at all latitudes

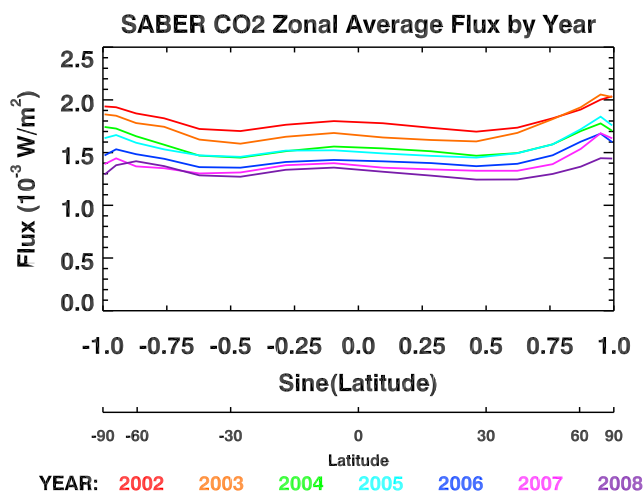


Figure 9. Annual average, zonal mean exiting longwave radiative flux (W m^{-2}) from carbon dioxide at $15 \mu\text{m}$ from 2002 to 2008.

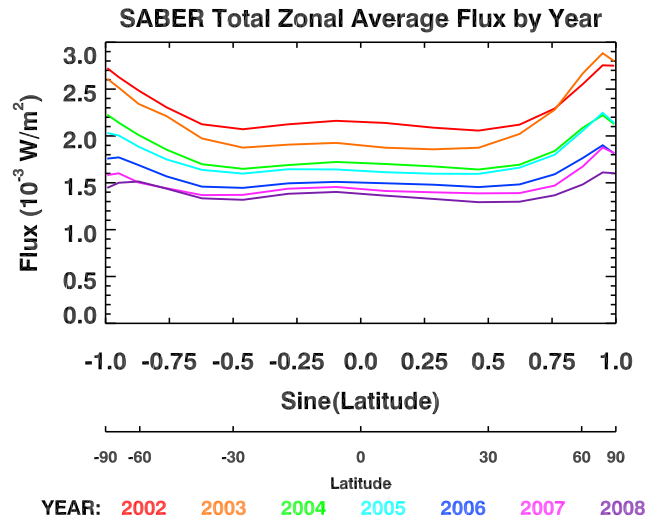


Figure 10. Annual average, zonal mean exiting longwave radiative flux, (W m^{-2}) for nitric oxide and carbon dioxide from 2002 to 2008.

indicates that the effects of solar variability are not necessarily uniform throughout the thermosphere.

[28] A second feature that stands out upon examination of Figures 8 and 9, and which is hinted at in Figures 1 and 2, is that the equator-to-pole gradient of the ELR is different for NO and CO_2 , with the gradient for NO being larger than for CO_2 . The equator-to-pole gradient of net heating (solar heating minus radiative cooling) of the atmosphere is a major factor that drives the large-scale circulation of the thermosphere, and the atmosphere in general. The fact that the gradient is larger in NO and becomes lesser over the solar cycle as both temperature and the NO abundance decrease implies a potential link between chemistry, dynamics, and radiation governed by the abundance of NO.

[29] Shown in Figure 10 is the zonally averaged ELR for the sum of NO and CO_2 . As shown for the individual ELR terms, the combined ELR is larger in all years at high latitudes than at low latitudes in both hemispheres. Because the ELR is the vertically integrated radiative cooling rate, the results illustrated in Figure 9 demonstrate that the high latitude and polar thermosphere is cooled more strongly by infrared radiation than at low and tropical latitudes. This result is fundamental. Larger radiative cooling at high latitudes than at low latitudes is known to exist in the mesosphere [Mlynckzak, 2000] and the stratosphere [Mlynckzak *et al.*, 1999]. However, in the troposphere, the opposite is true; that is, the OLR is larger at the equator than at the poles [Vonder Haar and Suomi, 1969]. The results of this and previous studies show that the upper atmosphere cools in a fundamentally different manner than the troposphere.

[30] Another property of the ELR evident from Figure 10 is that in addition to the general decrease in ELR over the 7 years of data, the equator-to-pole gradient of radiative cooling has weakened substantially over this time period. While the decrease in ELR implies that the thermosphere has cooled, and in the case of NO, that the abundance of NO has also likely decreased, the weakening of the equator-to-pole gradient of cooling implies that the large-scale dynamics may have also weakened considerably during this

SABER GLOBAL NO and CO₂ POWER, 100-200 km

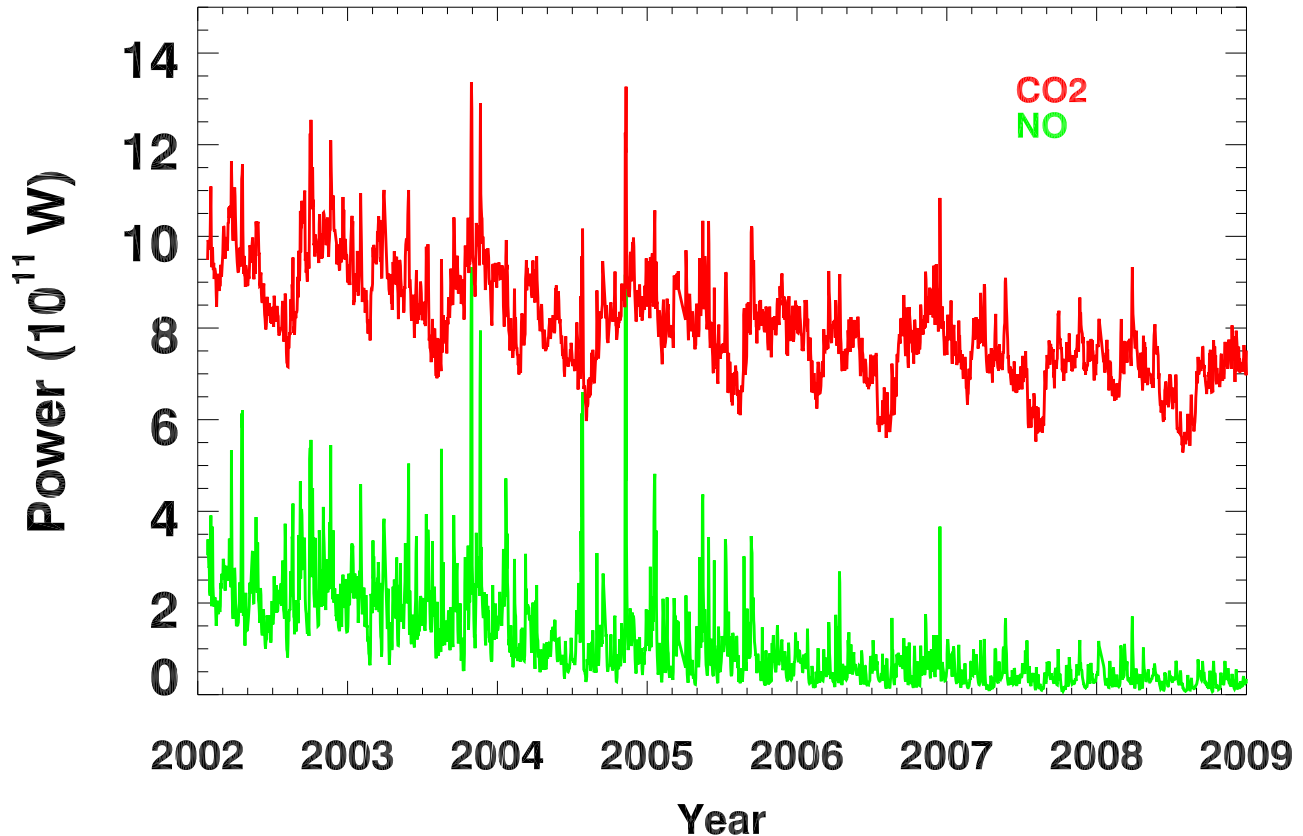


Figure 11. Daily global power (W) emitted from the thermosphere by CO₂ (red) and NO (green) between 100 km and 200 km altitude.

time. These infrared emissions thus provide solid evidence as to changes in the thermal structure, photochemistry, and dynamics of the thermosphere, and hint strongly at a coupling between NO chemistry and the large-scale dynamics and transport in the thermosphere.

3.4. Global Radiative Power

[31] The last parameter that we calculate is the global radiative power (W) emitted by CO₂ and NO. These have previously been shown by *Mlynczak et al.* [2007, 2008] in examining long- and short-term variations in the energy balance of the thermosphere. We obtain the total global power by zonally integrating the fluxes of ELR shown above, and then integrating the power in each latitude bin from pole to pole. To compute the power poleward of 55° in the hemisphere not being observed, we follow *Mlynczak et al.* [2005] in assuming the ratio of the power between the equator and 55° latitude and between 55° latitude and the pole is the same in both hemispheres. This process provides a measure of the total global power radiated by NO and CO₂ on a daily basis. The power for the full 7 years of data is shown in Figure 11. What is evident is the overall decline of radiated power consistent with the declining phase of solar cycle 23. In addition, there is substantial short-term variability in both the NO and CO₂ emissions that has previously been linked to geomagnetic phenomena [*Mlynczak et al.*, 2008]. Large increases in radiative power associated with

extreme geomagnetic events (e.g., the October 2003 Halloween superstorm event) are evident. In 2008, the values of NO power reach very low values, nearly a factor of 10 lower (when averaged over a 60 day yaw cycle) than at the beginning of the mission. During 2008, the Sun exhibited no sunspots for over 200 days. We suggest that the SABER data over this time period offer an excellent resource for studying the influence of the Sun on the climate of the upper atmosphere.

[32] The CO₂ cooling rates, fluxes of ELR, and radiative power shown above are all computed for the fundamental band of the CO₂ molecule. In the SABER temperature retrieval process more than 20 vibration-rotation bands (including isotopic bands) are considered and the non-LTE problem is solved for each band, including cooling rates in kelvin per day. To verify that the fundamental band dominates the CO₂ cooling we also computed cooling rates (W m⁻³), fluxes of ELR, and radiated power (W) for the first hot band of the CO₂ bending mode. Shown in Figure 12 is a time series of the power radiated by the CO₂ fundamental and first hot bands. It is clear from Figure 12 that the fundamental band dominates the CO₂ 15 μm thermospheric cooling and that the first hot band is about 3.5% of the fundamental band emission. However, the decrease in NO emission over the solar cycle is such that, between 100 and 200 km, the radiated power from the first hot band of CO₂ rivals that of NO in 2008, on an annual average basis,

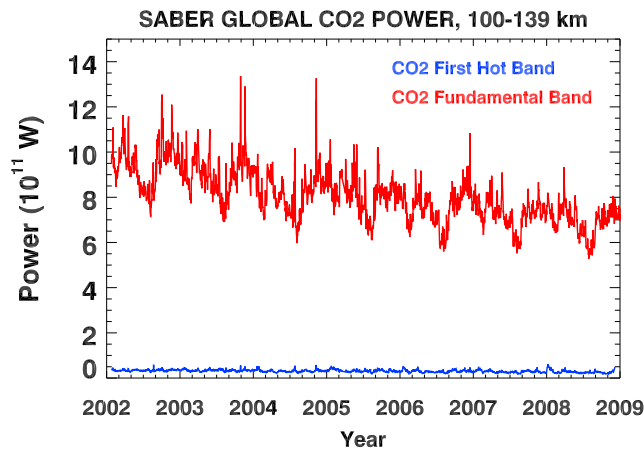


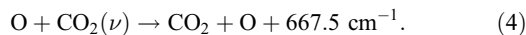
Figure 12. Daily global power (W) computed for CO₂ fundamental and first hot bands in the thermosphere between 100 km and 140 km.

although the emissions do peak in substantially different regions of the atmosphere. Table 1 lists the annual average power for CO₂ (fundamental and first hot bands) and NO for the 2002 through 2008 “yaw years.”

4. Sensitivity to Non-LTE Parameters in the SABER Algorithms

[33] A key question in the analysis and derivation of the CO₂ cooling rates in W m⁻³ is the extent to which the results are sensitive to the non-LTE processes and the modeling of these processes in the SABER temperature, pressure, and cooling rate (K d⁻¹) derivation in the operational SABER data processing algorithms. We demonstrate that the derived cooling rates, in W m⁻³, as a function of altitude, are essentially insensitive to the non-LTE parameters in the SABER algorithms, because the rate of emission is essentially constrained by the SABER radiance measurements. Furthermore, the ELR fluxes and radiated power are similarly insensitive since they are derived directly from the cooling rate in W m⁻³.

[34] The primary process by which CO₂ cools the atmosphere, analogous to NO, is by radiative emission subsequent to collisional excitation by an oxygen atom. In 1970, P. Crutzen postulated that this process would be important in cooling the thermosphere, and since that time, substantial efforts have been expended both in the laboratory [e.g., *Castle et al.*, 2006] and in analyzing atmospheric observations [e.g., *Rodgers et al.*, 1992; *López-Puertas et al.*, 1992] to determine the rate coefficient for the process,



Literature values for this “O/CO₂” rate coefficient range over a factor of 4 from approximately $6 \times 10^{-12} \text{ cm}^3 \text{ s}^{-1}$ [*Sharma and Wintersteiner*, 1990] to $\sim 1.4 \times 10^{-12} \text{ cm}^3 \text{ s}^{-1}$ [*Khvorostovskaya et al.*, 2002]. The SABER temperature algorithms incorporate the Sharma and Wintersteiner value for this rate coefficient.

[35] In the SABER algorithms, the modeling of the non-LTE processes depends on the provision of the O/CO₂ rate coefficient, the atomic oxygen density, and the CO₂ abundance. Atomic oxygen is provided from the NRL-MSIS

model [*Picone et al.*, 2002] and the CO₂ abundance is provided from the Whole Atmosphere Community Climate Model (WACCM) model (R. Garcia, National Center for Atmospheric Research, private communication, 2006). With these provisions, temperature is retrieved and constrained by the measured radiance at 15 μm by the SABER instrument [*Mertens et al.*, 2002].

[36] To assess the effect of the O/CO₂ rate coefficient on the derived cooling rates in W m⁻³ from CO₂, we ran 7 complete days of the v1.07 operational SABER algorithm in which we reduced the rate coefficient by a factor of 4 uniformly at all altitudes. This is also equivalent, in the non-LTE modeling, to varying the atomic oxygen concentration by a factor of 4, or the product of atomic oxygen and the rate coefficient by a factor of 4. We computed the cooling rates (W m⁻³), ELR fluxes (W m⁻²), and power (W) for each of the test days and compared to the original values. The results showed that the cooling rates (W m⁻³), fluxes, and power did not show much variation despite a huge variation in the key non-LTE rate coefficient. There are large changes in temperature, pressure, density, and cooling rates in kelvin per day, but not in the cooling rate in W m⁻³. An example is shown in Figure 13.

[37] The explanation for the relative insensitivity of the cooling rate (W m⁻³) is that decreasing the O/CO₂ rate coefficient results in a decrease in the population of excited CO₂ molecules in the algorithm. However, the SABER algorithm must compensate to match the measured radiance. It does this primarily by increasing the temperature and pressure. An increase in temperature increases the population of vibrationally excited CO₂ molecules by the Boltzmann factor as a consequence of detailed balance. The algorithm works to provide the correct number of excited CO₂ molecules to create the emission rate necessary to match the measured radiance. Thus, the cooling from CO₂ in W m⁻³ is essentially unchanged. Our approach is found to be quite robust and in fact provides the cooling rates (in W m⁻³) essentially independent of the non-LTE model parameters used to produce the SABER data products. The previously mentioned fact that radiative excitation from the lower atmosphere is not very large also contributes to this result. We note the NO cooling rates in W m⁻³ are also derived independent of any modeled non-LTE processes by virtue of the weak line inversion and because the NO emission is essentially generated solely by collisions with atomic oxygen.

[38] The relative insensitivity to non-LTE processes of the derived cooling rates in W m⁻³ presented here is a substantial result. The accuracy of the derived cooling rates is

Table 1. Annual Mean, Global Power (W) Radiated From the Thermosphere by the Carbon Dioxide Fundamental Band, the Carbon Dioxide First Hot Band, and by Nitric Oxide

Year	CO ₂ Fundamental Power (10 ¹¹ W)	CO ₂ First Hot Band Power (10 ¹¹ W)	NO ($\Delta\nu = 1$) Power (10 ¹¹ W)
2002	9.19	0.334	2.26
2003	8.85	0.332	1.94
2004	8.05	0.306	1.21
2005	7.69	0.306	0.947
2006	7.46	0.288	0.583
2007	6.97	0.267	0.407
2008	6.90	0.220	0.337

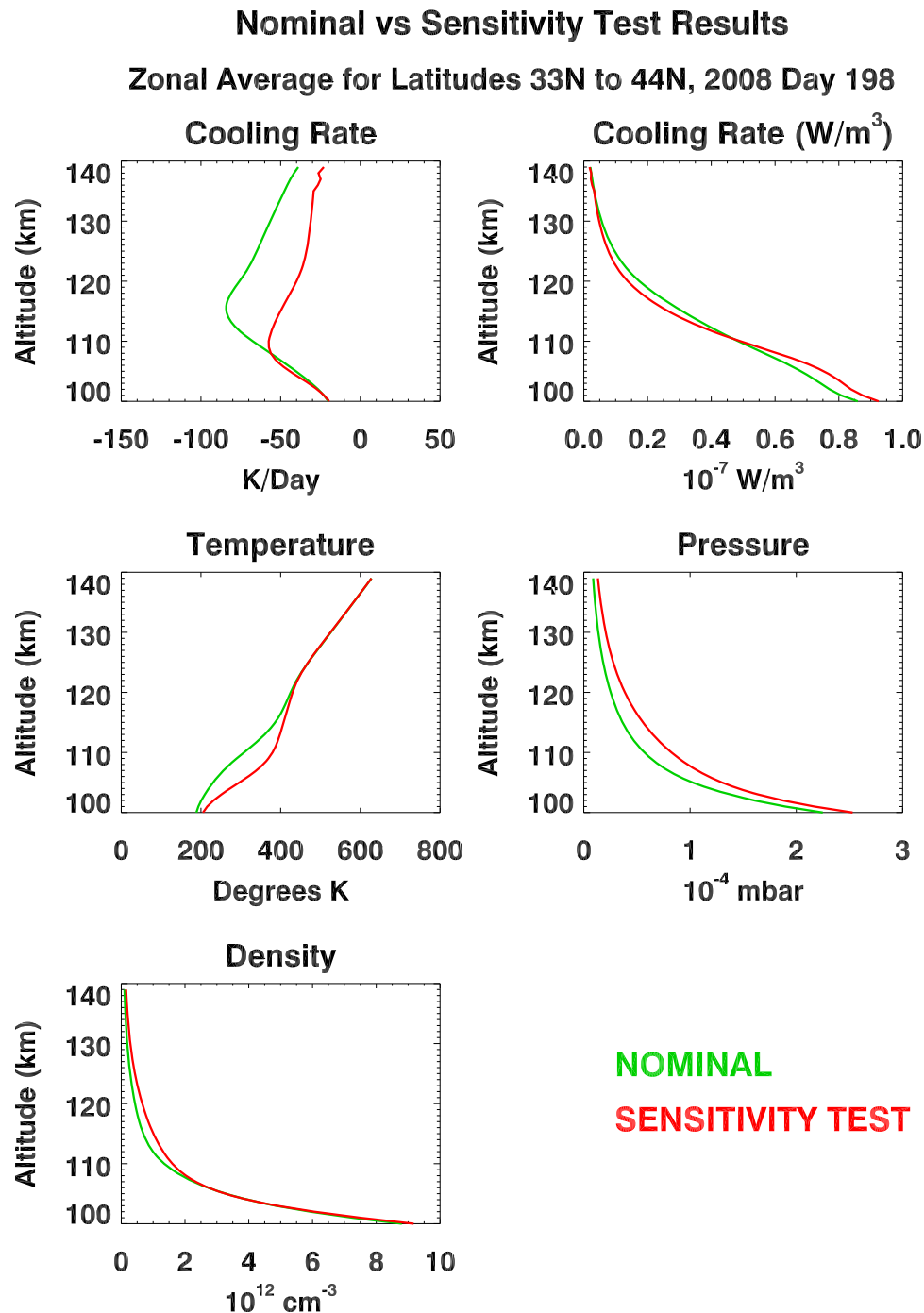


Figure 13. Results of SABER retrieved data products (radiative cooling rate in $K d^{-1}$, radiative cooling rate in $W m^{-3}$, kinetic temperature, pressure, and density), from the nominal retrieval algorithm (green) and from a sensitivity test in which the quenching rate of vibrationally excited carbon dioxide by atomic oxygen was reduced uniformly by a factor of 4 (red). The results show that the cooling rate in $W m^{-3}$ is essentially unchanged. See the text for further explanation.

then tied directly to the absolute calibration of the SABER instrument through the measured radiances. The cooling rates also represent a data set that can be used to test directly cooling rate parameterizations in upper atmosphere general circulation models (e.g., L. Qian and M.G. Mlynczak, submitted manuscript, 2010). The model parameterizations are very sensitive to the non-LTE processes including the

rate coefficient for energy transfer between atomic oxygen and carbon dioxide because they have no constraint (e.g., a measured radiance). Through such comparisons the long-standing discrepancies between renderings of the key non-LTE parameters may be resolved. The relative insensitivity to the large change in the rate coefficient also suggests that

the data set of cooling rates can form a climate data record [National Research Council, 2004] for the thermosphere.

5. Discussion and Summary

[39] We have presented 7 years of observations of the radiative cooling in the thermosphere as observed by the SABER instrument on the TIMED mission. The cooling rates in W m^{-3} are derived for emission from CO_2 at $15 \mu\text{m}$ and NO at $5.3 \mu\text{m}$. The emissions exhibit both short- and long-term variations that illustrate the sensitivity of the thermosphere on timescales ranging from daily to the 11 year solar cycle. The cooling by NO is substantially more variable than that of CO_2 due to a greater sensitivity to temperature and to a much larger variability of NO density with solar activity. Decreases in atomic oxygen between 2002 and 2008 likely contribute to the observed decrease in both NO and CO_2 cooling.

[40] The variability of the cooling has several fundamental consequences. First, the larger equator-to-pole gradient in cooling by NO , and its variability, implies a potential link to dynamics and transport as the equator-to-pole gradient in net heating drives the large-scale circulation. The observed weakening of the equator-to-pole gradient in radiative cooling over these 7 years is a strong indication that the large-scale thermospheric dynamics have also weakened. In addition, the larger cooling at the poles than at low latitudes in the thermosphere is consistent with the observed cooling in the mesosphere and stratosphere, but is opposite of what is observed in the troposphere. Thus the entire upper atmosphere behaves in a fundamentally different manner than the troposphere with regards to radiative cooling as a function of latitude.

[41] We have also shown that the cooling rates derived herein are essentially insensitive to the parameters and rate coefficients used to compute the non-LTE populations of the carbon dioxide molecule. This is because the retrieval algorithm must match the measured radiance, and thus will produce enough excited CO_2 molecules to accomplish this, whether by increasing temperature or pressure (or both) to accomplish the result. Further study on the sensitivity to the carbon dioxide abundance used in the retrieval is warranted. We would expect perhaps only minor sensitivity to CO_2 abundance given the relative insensitivity to a factor of 4 change in the primary process responsible for cooling, and we do not expect the CO_2 used in the SABER retrieval to be off by a factor of 4. At this time we estimate the cooling rates for CO_2 emission to be accurate to better than 15%.

[42] In the case of NO , the assumption is that the observed emission is essentially all cooling, and that the Abel inversion and correction factors applied to determine the total band emission are sufficient. There are uncertainties in the derived cooling, most notably in the process used to derive the full band cooling from the measured in-band emission. This correction (“unfilter”) factor is essentially a function of the rotational temperature of the NO vibration-rotation bands. For the v1.07 SABER data we do not make a correction for the rotational temperature as a function of time. As the thermosphere cools, we would expect the rotational temperature to decrease and thus there is a possibility that the correction factor to generate the total cooling rates would also change. If that were the case, the correction factor

would in general decrease, implying that the changes with solar cycle may be larger than that presented above. These possibilities will be investigated in future studies by the SABER science team. We also estimate the cooling rates due to NO to be accurate to better than 15%. This estimate is based on the accuracy of the SABER radiometric calibration (1%), the possible effects of rotational temperature uncertainties ($\sim 10\%$), and on emissions that may not be properly accounted for in correcting for the spectral response filter function of the SABER NO channel ($\sim 10\%$). Assuming these uncertainties are uncorrelated, the root sum square of these is conservatively $\sim 15\%$.

[43] In closing we suggest that the data set of radiative cooling of the thermosphere by NO and CO_2 constitutes a first climate data record for the thermosphere. The length of the data record and the apparent lack of dependence of the data products on model parameters results in an accurate set of parameters that can be used to conduct fundamental tests of general circulation models of the thermosphere. The cooling rates, radiative fluxes, and radiated power can all be compared with model calculations. This should enable tests of model chemistry and physics and in principle, resolve long-standing issues with regards to the parameterization of radiative cooling in these models. As the TIMED mission continues, these data derived from SABER will become important in assessing long-term changes due to the increase of carbon dioxide in the atmosphere.

[44] **Acknowledgments.** M.G.M. would like to acknowledge continued support from the Science Directorate at NASA Langley, from the NASA Heliophysics Division TIMED Project, and from the NASA Heliophysics Division Guest Investigator Program.

[45] Zuyin Pu thanks Bernd Funke and another reviewer for their assistance in evaluating this paper.

References

- Bates, D. R. (1951), The temperature of the upper atmosphere, *Proc. Phys. Soc.*, *B64*, 805–821.
- Castle, K. J., K. M. Kleissas, J. M. Rhinehart, E. S. Hwang, and J. A. Dodd (2006), Vibrational relaxation of $\text{CO}_2(\nu_2)$ by atomic oxygen, *J. Geophys. Res.*, *111*, A09303, doi:10.1029/2006JA011736.
- Curtis, A. R., and R. M. Goody (1956), Thermal radiation in the upper atmosphere, *Proc. R. Soc. Ser. A*, *236*, 193–206, doi:10.1098/rspa.1956.0128.
- Dothe, H., J. W. Duff, R. D. Sharma, and N. B. Wheeler (2002), A model of odd nitrogen in the aurorally dosed nighttime terrestrial thermosphere, *J. Geophys. Res.*, *107*(A6), 1071, doi:10.1029/2001JA000143.
- Funke, B., and M. López-Puertas (2000), Nonlocal thermodynamic equilibrium vibrational, rotational, and spin state distribution of $\text{NO}(v = 0, 1, 2)$ under quiescent atmospheric conditions, *J. Geophys. Res.*, *105*, 4409–4426.
- Gardner, J. L., B. Funke, M. G. Mlynarczyk, M. López-Puertas, F. J. Martín-Torres, J. M. Russell III, S. M. Miller, R. D. Sharma, and J. R. Winick (2007), Comparison of nighttime nitric oxide $5.3 \mu\text{m}$ emissions in the thermosphere measured by MIPAS and SABER, *J. Geophys. Res.*, *112*, A10301, doi:10.1029/2006JA011984.
- Grossman, K. U., and K. Vollmann (1997), Thermal infrared measurements in the middle and upper atmosphere, *Adv. Space Res.*, *19*(4), 631–638, doi:10.1016/S0273-1177(97)00156-7.
- Grossman, K. U., M. Kaufmann, and E. Gerstner (2000), A global measurement of lower thermosphere atomic oxygen densities, *Geophys. Res. Lett.*, *27*, 1387–1390, doi:10.1029/2000GL003761.
- Hwang, E. S., K. J. Castle, and J. A. Dodd (2003), Vibrational relaxation of $\text{NO}(v = 1)$ by oxygen atoms between 295 and 825 K, *J. Geophys. Res.*, *108*(A3), 1109, doi:10.1029/2002JA009688.
- Khvorostovskaya, L. E., I. Y. Potekhin, G. M. Shved, V. P. Ogibalov, and T. V. Uzyukova (2002), Measurement of the rate constant for quenching CO_2 [0110] by atomic oxygen at low temperatures: Reassessment of the

- rate of cooling by the CO₂ 15- μ m emission in the lower thermosphere, *Atmos. Ocean. Phys.*, **38**, 613–624.
- Kockarts, G. (1980), Nitric oxide cooling in the terrestrial thermosphere, *Geophys. Res. Lett.*, **7**, 137–140, doi:10.1029/GL007i002p00137.
- López-Puertas, M., and F. Taylor (2002), *Non-LTE Radiative Transfer in the Atmosphere*, Ser. Atmos., Ocean Planet. Phys., vol. 3, World Sci., Singapore.
- López-Puertas, M., R. Rodrigo, A. Molina, and F. W. Taylor (1986a), A non-LTE radiative transfer model for infrared bands in the middle atmosphere, I. Theoretical basis and application to the CO₂ 15 μ m bands, *J. Atmos. Terr. Phys.*, **48**, 729–748, doi:10.1016/0021-9169(86)90022-X.
- López-Puertas, M., R. Rodrigo, J. J. López-Moreno, and F. W. Taylor (1986b), A non-LTE radiative transfer model for infrared bands in the middle atmosphere, II, CO₂ (2.7 and 4.3 μ m) and water vapour (6.3 μ m) and N₂(1) and O, *J. Atmos. Terr. Phys.*, **48**, 749–764, doi:10.1016/0021-9169(86)90023-1.
- López-Puertas, M., M. A. López-Valverde, C. P. Rinsland, and M. R. Gunson (1992), Analysis of the upper atmospheric CO₂ (ν_2) vibrational temperatures retrieved from ATMOS-Spacelab 3 observations, *J. Geophys. Res.*, **97**, 20,469–20,478.
- Mertens, C. J., M. G. Mlynczak, M. López-Puertas, and E. E. Remsberg (2002), Impact of non-LTE processes on middle atmospheric water vapor retrievals from simulated measurements of 6.8 μ m Earth limb emission, *Geophys. Res. Lett.*, **29**(9), 1288, doi:10.1029/2001GL014590.
- Mlynczak, M. G. (1996), Energetics of the middle atmosphere: Theory and observation requirements, *Adv. Space Res.*, **17**(11), 117–126, doi:10.1016/0273-1177(95)00739-2.
- Mlynczak, M. G. (1997), Energetics of the mesosphere and lower thermosphere and the SABER experiment, *Adv. Space Res.*, **20**(6), 1177–1183, doi:10.1016/S0273-1177(97)00769-2.
- Mlynczak, M. G. (2000), A contemporary assessment of the middle atmosphere energy budget, in *Atmospheric Science Across the Stratopause*, *Geophys. Monogr. Ser.*, vol. 123, edited by D. Siskind et al., pp. 37–52, AGU, Washington, D. C.
- Mlynczak, M. G., C. J. Mertens, R. R. Garcia, and R. W. Portmann (1999), A detailed evaluation of the stratospheric heat budget: 2. Global radiation balance and diabatic circulations, *J. Geophys. Res.*, **104**, 6039–6066, doi:10.1029/1998JD200099.
- Mlynczak, M., et al. (2003), The natural thermostat of nitric oxide emission at 5.3 μ m in the thermosphere observed during the solar storms of April 2002, *Geophys. Res. Lett.*, **30**(21), 2100, doi:10.1029/2003GL017693.
- Mlynczak, M. G., F. J. Martin-Torres, D. G. Johnson, D. P. Kratz, W. A. Traub, and K. Jucks (2004), Observations of the O(³P) fine structure line at 63 μ m in the upper mesosphere and lower thermosphere, *J. Geophys. Res.*, **109**, A12306, doi:10.1029/2004JA010595.
- Mlynczak, M. G., et al. (2005), Energy transport in the thermosphere during the solar storm events of April 2002, *J. Geophys. Res.*, **110**, A12S25, doi:10.1029/2005JA011141, (Correction, *J. Geophys. Res.*, **112**, A02303, doi:10.1029/2006JA012008, 2007.)
- Mlynczak, M. G., F. J. Martin-Torres, B. T. Marshall, E. Thompson, J. Williams, T. Turpin, D. P. P. Kratz, J. M. Russell III, T. N. Woods, and L. L. Gordley (2007), Evidence for a solar cycle influence on the infrared energy budget and radiative cooling of the thermosphere, *J. Geophys. Res.*, **112**, A12302, doi:10.1029/2006JA012194.
- National Research Council (2004), *Climate Data Records From Environmental Satellites*, Natl. Acad. Press, Washington, D. C.
- Picone, J. M., A. E. Hedin, D. P. Drob, and A. C. Aikin (2002), NRLMSISE-00 empirical model of the atmosphere: Statistical comparisons and scientific issues, *J. Geophys. Res.*, **107**(A12), 1468, doi:10.1029/2002JA009430.
- Rodgers, C., F. Taylor, A. Muggeridge, M. López-Puertas, and M. López-Valverde (1992), Local thermodynamic equilibrium of carbon dioxide in the upper atmosphere, *Geophys. Res. Lett.*, **19**, 589–592, doi:10.1029/92GL00160.
- Russell, J. M., III, M. G. Mlynczak, L. L. Gordley, J. J. Tansock Jr., and R. W. Esplin (1999), Overview of the SABER experiment and preliminary calibration results, *Proc. SPIE*, **3756**, 277, doi:10.1117/12.366382.
- Sharma, R., and P. Wintersteiner (1990), Role of carbon dioxide in cooling planetary thermospheres, *Geophys. Res. Lett.*, **17**, 2201–2204, doi:10.1029/GL017i012p02201.
- Sharma, R. D., H. Dothe, F. von Esse, V. A. Kharchenko, Y. Sun, and A. Dalgarno (1996), Production of vibrationally and rotationally excited NO in the night time terrestrial thermosphere, *J. Geophys. Res.*, **101**, 19,707–19,713.
- Vonder Haar, T. H., and V. E. Suomi (1969), Measurements of the Earth's radiation budget from satellites during a five-year period: Part I. Extended time and space means, *J. Atmos. Sci.*, **28**, 305–314, doi:10.1175/1520-0469(1971)028<0305:MOTERB>2.0.CO;2.
- L. L. Gordley, R. E. Thompson, and B. Thomas Marshall, GATS Inc., 11864 Canon Blvd., Ste. 101, Newport News, VA 23606, USA.
- L. A. Hunt, SSAI, 1 Enterprise Pkwy., Ste. 200, Hampton, VA 23666, USA.
- M. López-Puertas, IAA, E-18008 Granada, Spain.
- F. J. Martin-Torres, Jet Propulsion Laboratory, California Institute of Technology, Pasadena, CA 91109, USA.
- C. J. Mertens, M. G. Mlynczak, and E. E. Remsberg, NASA Langley Research Center, Hampton, VA 23681, USA. (m.g.mlynczak@nasa.gov)
- R. Picard and J. Winick, AFRL, Hanscom AFB, 29 Randolph Rd., Bedford, MA 01731, USA.
- J. M. Russell III, Hampton University, Hampton, VA 23668, USA.
- P. Wintersteiner, ARCON Corp., 260 Bear Hill Rd., Waltham, MA 02451, USA.